Received: 8 June 2021 | Revised: 7 September 2021 | Accepted: 29 November 2021 | Published on: 15 December 2021

DOI: 10.1002/joc.7483

RESEARCH ARTICLE

International Journal of Climatology RMetS

Super droughts over East Asia since 1960 under the impacts of global warming and decadal variability

Lin Wang[1] | Wen Chen[2,3] | Qiang Fu[4] | Gang Huang[3] | Qiulin Wang[3] | Chakrit Chotamonsak[5] | Atsamon Limsakul[6]

[1]CAS Key Laboratory of Regional Climate-Environment for Temperate East Asia, Institute of Atmospheric Physics, Chinese Academy of Sciences, Beijing, China

[2]Center for Monsoon System Research, Institute of Atmospheric Physics, Chinese Academy of Sciences, Beijing, China

[3]State Key Laboratory of Numerical Modeling for Atmospheric Sciences and Geophysical Fluid Dynamics, Institute of Atmospheric Physics, Chinese Academy of Sciences, Beijing, China

[4]Department of Atmospheric Sciences, University of Washington, Seattle, Washington, USA

[5]Department of Geography, Faculties of Social Sciences, Chiang Mai University, Chiang Mai, Thailand

[6]Environmental Research and Training Center, Klong Luang, Thailand

Correspondence

Lin Wang and Gang Huang, Institute of Atmospheric Physics, Chinese Academy of Sciences, Beijing 100029, China.
Email: linwang@mail.iap.ac.cn or wang_lin@mail.iap.ac.cn (L. W.) and
Email: hg@mail.iap.ac.cn (G. H.)

Funding information

National Natural Science Foundation of China, Grant/Award Numbers: 41961144016, 41875115, 42175041, 41961144025, 41831175

Abstract

In the last decade, a sequence of once-in-50 year or even once-in-100 year high-impact drought events have hit East Asia. By defining a super drought with the Standardized Precipitation Evaporation Index for the time scales of 3, 6, 12 and 24 months all below −1.5, this study aims to examine the changes in super droughts and the underlying mechanism over East Asia in the past 60 years, putting the recent high-impact droughts in the context. Super droughts in the last 10 years over East Asia have been the most expansive, with two hotspots located in the Transitional Climate Zone (TCZ) and the Southeast Asian region (SEA) regions, together accounting for 2/3 of the total. The seasonal distribution characterizes the largest contribution from summer followed by autumn and then spring and winter. Super droughts over TCZ peak in the recent two decades, which are primarily driven by the increase in potential evaporation (PET) contributing 41 and 80% in the first and second 10 years, respectively. It turns out that global warming signal can explain more than 90% of this PET increase. Over SEA, the recent decade and the period around 1990 saw the most widespread super droughts that were not spatially uniformly distributed but clustered in three subregions. Different from TCZ, the precipitation rather than PET is the most influential in governing super droughts over SEA. Out of the total variability in precipitation, about half of the super droughts in the recent decade is caused by decadal variability, while the trend mode has negligible influence.

KEYWORDS

attribution, detection, East Asia, extreme event, Southeast Asian region, super drought, Transitional Climate Zone

1 | INTRODUCTION

The global population affected by drought in the first 20 years of the 21st century is estimated to be 1.43 billion, which is second only to flood (1.65 billion), according to recently published report "Human Cost of Disasters 2000–2019" compiled by the UN Office for Disaster Risk Reduction (2020). Drought is likely the most complex natural hazard due to its elusive, wide-ranging and cascading impacts that permeate all areas of our lives (WMO, 2006). Under the background of global warming, there is growing evidence that the world will experience more frequent and more exceptional drought and aridity (Feng and Fu, 2013; Fu and Feng, 2014; Sherwood and

Fu, 2014; Huang *et al.*, 2016; Zhang *et al.*, 2017; Guan *et al.*, 2019; Zhao and Dai, 2017).

Asia, particularly China, is one of the drought-prone regions, due to the complex land surface conditions and monsoon climate dynamics (Chen *et al.*, 2013; Wang *et al.*, 2013; Chen *et al.*, 2019a; He and Zhou, 2020). The drought occurrence and durations in East Asia show an increasing tendency during the past 50 years (Zhang and Zhou, 2015), which is projected to continue throughout the 21st century (Wang and Chen, 2014; Wang *et al.*, 2014; Spinoni *et al.*, 2020). In particular, the recent decades have witnessed a number of unprecedented once-in-50 year or once-in-100 year drought events, for example, the recurrent southwest China droughts since the summer of 2006, the 2014–2015 drought years in Southeast Asia, the Mongolian drought in 2017 and the recent decade long drought in northeast India (Li *et al.*, 2011; Barriopedro *et al.*, 2012; Parida and Oinam, 2015; Wang *et al.*, 2015; FAO, 2017; Piao *et al.*, 2017; United Nations ESCAP, 2019; Ding and Gao, 2020). These droughts have resulted in tremendous losses, including a lack of drinking water, ecosystem destruction, crop failure, health problems and even human mortality.

Wang *et al.* (2016) highlighted that the historically unprecedented drought is not traditionally articulated as but in fact super drought, which is characterized by a combination of extremely dry states in multiple components of water resources. A lot of studies have been dedicated to investigating the characteristics and physical mechanisms linked to a specific super drought event, despite not being explicitly framed as super drought, with a focus on case studies (e.g., Li *et al.*, 2011; Barriopedro *et al.*, 2012; Parida and Oinam, 2015; Sun *et al.*, 2019; Ding and Gao, 2020; Wang *et al.*, 2021). However, most research has been centred on case studies. Thus, there is an urgent need to advance our understanding of super drought changes over East Asia in the context of long-term historical perspective. How has super drought changed since 1960 over East Asia and how was the super drought in the last two decades compared to the preceding decades? Where are the hotspots frequently struck by super drought? What are the climatic driving factors? To what extent is the super drought governed by internal decadal variability or long-term trend associated with global warming?

In this paper, we detected super drought hotspots over East Asia since 1960, disclosed the climatic driving factors, and examined how much of the change can be attributed to ongoing trend and how much can be attributed to internal decadal variability. The overall structure is arranged as follows. Section 2 describes the data and methods. The detection and attribution of super drought hotspot over East Asia are presented in section 3 and section 4, respectively. Section 5 summarizes the main conclusions.

2 | DATA AND METHODS

2.1 | Data

2.1.1 | Observational data

Monthly precipitation and potential evaporation (PET, units: mm) are obtained from the latest version TS4.04 of Climatic Research Unit (Harris *et al.*, 2020). The CRU PET is derived based on Penman–Monteith scheme (Allen *et al.*, 1994). These data are available at $0.5^\circ \times 0.5^\circ$ horizontal resolution and extends over the global land. Given the relatively poor quality and low spatial density of in situ measurements in the earlier part of the twentieth century, the data records from 1950 onwards are used. Meanwhile, in order to focus on the East Asia region, the spatial domain is chosen to be from 0°N to 60°N and from 70°E to 150°E.

To verify the drought signatures revealed by drought index, the soil moisture data from Global Land Data Assimilation System Version 2 (GLDAS) are used (Rodell *et al.*, 2004). GLDAS-2 has three components: GLDAS-2.0, GLDAS-2.1 and GLDAS-2.2. GLDAS-2.0 is forced entirely with the Princeton meteorological forcing input data and provides a temporally consistent series from 1948 through 2014 (Beaudoing and Rodell, 2019). GLDAS-2.1 is forced with a combination of model and observation data from 2000 to present (Beaudoing and Rodell, 2020). To match the time span of the drought index, we concatenate GLDAS-2.1 data over 1948–1999 and GLDAS-2.2 over 2000–2019 at monthly interval. Soil moisture are provided at four vertical layers: 0–10 cm, 10–40 cm, 40–100 cm and 100–200 cm.

Ancillary data including global topography and land type are employed. ETOPO 1 arc-minute gridded elevation data (Amante and Eakins, 2009) from NOAA are used to mask out the Tibetan Plateau that has its own unique climate characteristics and thus is not considered in this study. The global land cover map V2.3 compiled by European Space Agency (http://due.esrin.esa.int/page_globcover.php) are used to exclude desert areas. This is because it is problematic to calculate drought indices in the presence of high frequency of near-zero values (Vicente-Serrano *et al.*, 2015) and calculating drought indices in desert areas is also meaningless. The topography and land type data are all converted to the CRU $0.5^\circ \times 0.5^\circ$ resolution using a nearest-neighbour interpolation.

2.1.2 | CMIP6 model data

The attribution analysis with model data in the framework of the phase 6 of the Coupled Model Intercomparison

Project (CMIP6) is carried out to verify the results based on observational data. We use the following experiments from CMIP5: the preindustrial control simulation (piControl) and 1850–2014 full-forcing historical simulation (Hist). To match the time span of observation, the SSP2-4.5 scenario data for 2015–2019 are appended to the Hist data. Only one realization member is employed for each model. Variables directly used from the CMIP6 monthly model output included precipitation, near-surface mean, minimum and maximum air temperature, surface pressure, wind speed at 10 m, precipitation, surface downwelling shortwave radiation, surface upwelling shortwave radiation, surface downwelling longwave radiation, surface upwelling longwave radiation, and near-surface relative humidity. All above variables other than precipitation are needed in PET calculation. The attribution analyses for precipitation and PET use slightly different sets of models, due to the availability of required variables and time coverage. There are totally 32 models used for precipitation attribution, and Table S1 lists the model names and length of piControl run. In parallel, Table S2 provides the list of datasets that will be used in PET attribution. The abbreviations for above variables are also shown in Table S2.

2.2 | Methods

2.2.1 | Multiscalar drought and Standardized Precipitation Evaporation Index

It is broadly accepted that drought is intrinsically a multiscalar phenomenon (Hayes *et al*., 2011). Standardized Precipitation Evaporation Index (SPEI) and its predecessor Standardized Precipitation Index (SPI) can be calculated across a spectrum of time scales, which is essential for capturing drought impact on different usable water resources and differentiating among different drought types involving meteorological, agricultural and hydrological drought (McKee et al., 1993; Vicente-Serrano *et al*., 2010). Compared to SPI depending on precipitation alone, SPEI is built to take the atmospheric evaporative demand into account, making it more relevant for drought assessment in the context of global warming. In this study, the SPEI is computed at time scales of 3, 6, 12 and 24 months, with the calibration period of 1960–1999 being used. The detailed algorithm can be found in Beguería *et al*. (2014).

2.2.2 | Super drought

This study is centred at the devastating high-impact drought but how should such event be defined? In traditional way, a drought can usually be categorized as a "severe" or "extreme" one based on the magnitude of anomalous values of drought index. Taking SPEI for example, a severe/extreme drought happens when the index reaches a value equal to or less than −1.5/−2. However, the so-called "severe" or "extreme" category here might not be a proper indicator of high-impact drought. This is because droughts often occur on multiple time scales, and it is common to find severe or extreme conditions at one time scale but normal or even humid conditions at other time scales (Vicente-Serrano *et al*., 2015). As such, the categorization of severe or extreme drought should only be referred to a particular time scale, or part of hydrological cycle.

Wang *et al*. (2016) proposed the concept of super drought, referring to the simultaneous occurrence of severe/extreme droughts at multiple time scales, noting that the damage resulting from the drought events on different time scales would reinforce each other. They defined a super drought when SPEI is below −1.5 at several representative time scales, which are chosen to span the range of short-, medium- and long-time scales. In physical sense, super drought can be regarded as the pronounced loss in total rather than part of usable water storage, or in other words the combination of multiple stresses on water resources. The real world assessment highlights that the defined super drought captures well the actual reported devastating drought but excludes inconsequential ones, while the traditional measure fails to deliver. Moreover, the super drought is further divided into two classes: one is SE-type with representative SPEIs all below −1.5, and the other is E-type with those all below −2. In this study, we examine SE-type rather than E-type super drought in the analyses, because E-type super drought only has a 0.1% chance of happening and thereby no sufficient samples are available for robust statistical inferences. The details about super drought concept including motivation, physical significance, real-world verification can be found in Wang *et al*. (2016).

2.2.3 | Estimation of the forced long-term trends and internal decadal variability

There are generally two families of methods to disentangle the externally forced long-term trend and internal variability, one relying solely on observation and the other involving climate model simulation (Frankignoul *et al*., 2017; Chen *et al*., 2019b). On the one hand, approaches only rely on observations include linear trend, quadratic trend, global mean, regression on global mean, empirical mode decomposition (EMD). On the other hand, the relative contribution of external forcing and internal variability can be assessed through the use of ensembles of climate model simulations (Chen and Sun, 2017; Ma *et al.*, 2017; Zhang *et al.*, 2017; Li *et al.*, 2020; Zhang *et al.*, 2020).

In this study, the empirical mode decomposition (EMD) method is adopted as the primary method to separate the long-term trends and internal decadal variability. EMD was originally proposed by Huang *et al.* (1998) to decompose the signal into intrinsic mode functions (IMFs) and to separate short timescale signals from a general trend, and has becomes a popular technique in climate science communities. To avoid mode mixing issues, Wu and Huang (2009) developed Ensemble EMD (EEMD), which is an ensemble of EMD trials obtained by adding finite amplitude normally distributed white noise to the time series prior to each EMD run. Even so, signals with added noise can produce a large number of iterations in the EEMD process, and signal result holds residual noise after decomposition. Torres *et al.* (2011) resolved the downsides of EEMD with a variant denoising method, called Complete EEMD with Adaptive Noise (CEEMDAN), which yields an exact reconstruction of the original signal and a cleaner spectral separation of modes. In this study, CEEMDAN is used; unless otherwise stated, the term EMD is used to refer to CEEMDAN.

To verify the results obtained by EMD analysis for the observation, we employ the ensemble from the CMIP6). For precipitation, we use the same method in Zhang *et al.* (2021) to explore the role of external-imposed trend and internal decadal variability, based on the comparison of the piControl and Hist simulation. Specifically, the internal decadal variability is estimated from piControl, which is defined as the range between the maximum and minimum values across the entire piControl runs. Prior to the calculation, the 20-year running mean is first applied. Meanwhile, the multimodel ensemble mean (MME) in Hist is calculated to denote the external forcing. Note that we do not simply follow Zhang *et al.* (2021) but instead getting a different perspective on the precipitation attribution.

Compared to precipitation, ubiquitous increases in PET are found over global land which is directly driven by anthropogenic global warming (Sherwood and Fu, 2014). Hence, we use the Dai *et al.* (2015) method which assumes the global-mean ensemble-mean time series of surface temperature can be used to represent the temporal structure of the true forced response, but we extend the approach to PET. Specifically, the forced signal is estimated by linear regression of local observed PET onto the global mean PET time series from the CMIP6 Hist ensemble mean, while the internally generated variability is derived by subtracting the forced changes from the local observed PET. Both observed and model series have been pre-smoothed by 5-point running mean. The Dai *et al.* (2015) method can tell the decadal phase, as it involves observational signal, which is difficult for exclusively model-dependent. However, the assumption of Dai *et al.* (2015) may not be held for precipitation, because the global mean can hardly represent the forced behaviour at local scale. That is why we do not apply the method to precipitation attribution.

2.2.4 | PET estimate

The PET in CMIP6 is parameterized through Penman–Monteith scheme (Allen *et al.*, 1994), which accounts for the combined effects of temperature, radiation, humidity and wind speed. The mathematical form of Penman–Monteith can be found in Allen *et al.* (1994) and Wang *et al.* (2014). The direct input to calculate PET involves net radiation at surface, air temperature at 2 m height, wind speed at 2 m height, saturation vapour pressure, actual vapour pressure, slope of saturation vapour pressure curve, psychrometric constant and soil heat flux. When working with CMIP6 model output, the above parameters are obtained as follows: the net radiation is calculated by rsds−rsus+rlds−rlus, air temperature at 2 m height is directly at hand, wind speed at 10 m height is converted to 2 m height based on based on a logarithmic wind profile, saturation vapour pressure and slope of saturation vapour pressure curve are dependent on air temperature, actual vapour pressure is calculated based on daily minimum and maximum temperature along with mean relative humidity, psychrometric constant is estimated from surface pressure, and soil heat flux is derived from the mean air temperature of the previous and next month. Considering some input parameters required by Penman–Monteith computation are not available in some models (see Table S2), we first derive the ensemble mean for each required variable prior to calculating PET.

3 | SPATIAL AND TEMPORAL DETECTION OF SUPER DROUGHTS

3.1 | Super drought hotspots identification

Figure 1 shows the spatial distribution of the super drought numbers per decade and the summation of these numbers over all grid pixels for each decade from 1960 to 2019. Here, each touch of super drought threshold in one grid cell and 1 month is counted as one occurrence. Before the turn-of-the-century, the East Asia experiences low occurrences of super drought, and the affected areas

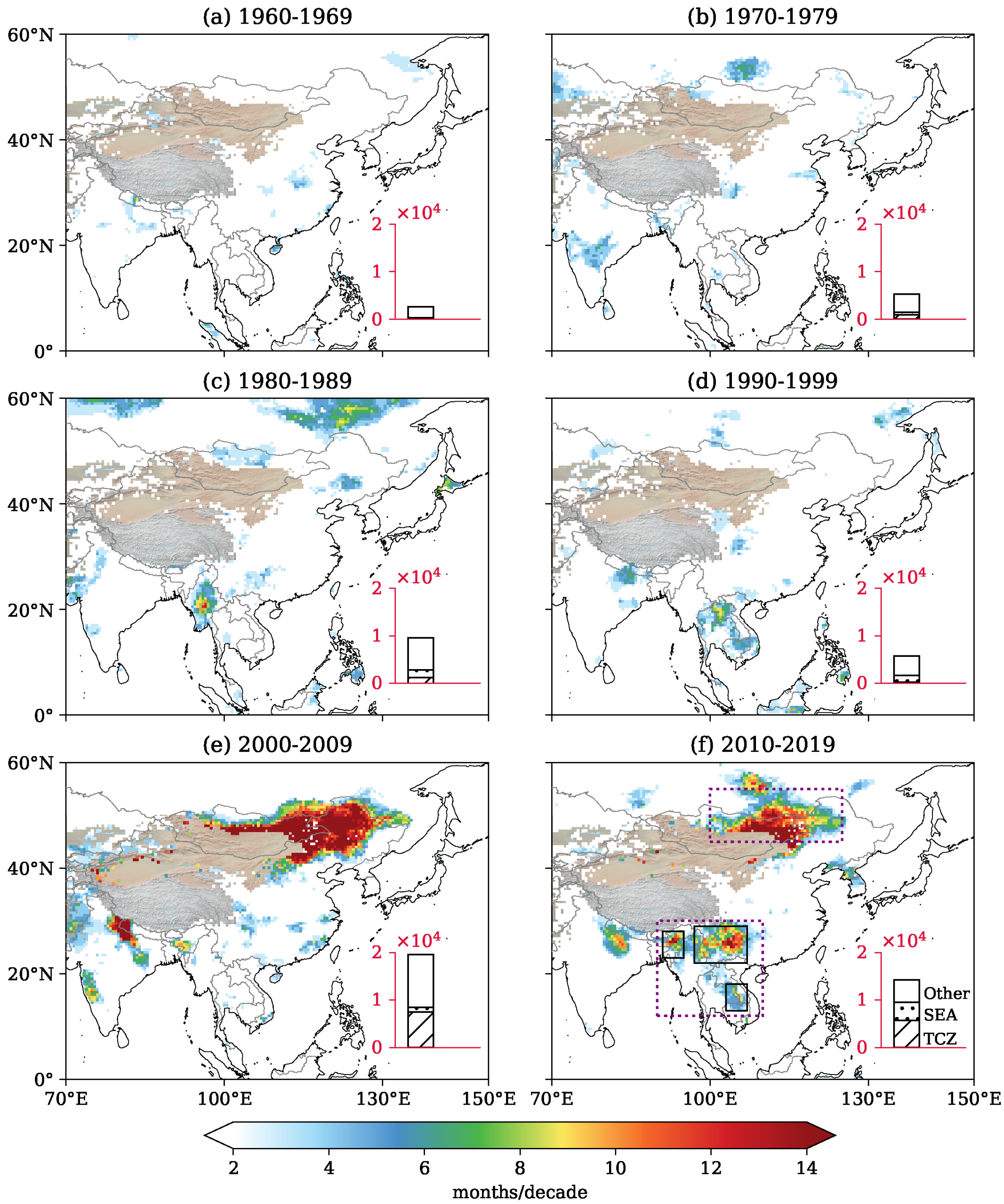

FIGURE 1 Spatial distribution of number of months under super drought for six consecutive decades (a) 1960–1969, (b) 1970–1979, (c) 1980–1989, (d) 1990–1999, (e) 2000–2009, (f) 2010–2019 with a horizontal resolution of 0.5° × 0.5°. The purple-dotted boxes denotes Transitional Climate Zone (TCZ) in the north and Southeast Asian region (SEA) in the south. The inset in the bottom right illustrates the total number of super droughts over all grid points and its contribution from TCZ, SEA and other regions. Tibetan Plateau and desert areas, indicated by grey and light brown colours, respectively, are excluded in the analyses [Colour figure can be viewed at wileyonlinelibrary.com]

are rather scattered. However, the total number of super drought occurrences has sharply increased to 2×10^4 and 1.4×10^4 counts/decade over the last two decades from below 10^4 counts/decade before 2000. Not only did the incidence of the super drought increase, but also its geographical coverage. Two super drought hotspots, located in the Transitional Climate Zone (TCZ, 45°–55°N and 100°–125°E) in the north and the Southeast Asian region (SEA, 12°–30°N and 90°–110°E) in the south, stand out in the last decade (i.e., 2010–2019) when TCZ and SEA contribute 40 and 27% of the total amount, respectively, together accounting for 2/3 of the total. On the one hand, note that the TCZ hotspot delimited here is actually the north branch of the entire TCZ domain over East Asia, which geographically stretches in a northeast–southwest orientation from the eastern fringe of Tibetan Plateau to the eastern Mongolia (Wang *et al*., 2017; 2020). For simplicity, we refer this region as TCZ. On the other hand, the term SEA is used here to cover the Indo-China Peninsula, southwest China and northeast India, in order to be differentiating with the term Southeast Asia which is mainly referred to the Indo-China Peninsula.

Super drought condition in TCZ peaks in 2000–2009, representing about one-half of the East Asian total, which was followed by a slightly recovery in the subsequent decade. Over the SEA, it reveals unprecedented widespread, intense super droughts in the recent decade, which is more severe than any decades in the past 60 years. Compared to TCZ, super drought change is not uniform across the SEA, but clustered into the following subregions: southwest China (SWC) (22°–29°N, 97°–107°E), Indochinese Peninsula (ICP) (13°–18°N, 97°–107°E) and northeast India (NEI) (23°–28°N, 91°–95°E) (see black boxes in Figure 1f). The spatial distributions of E-type super drought shown for six decades (Figure S1) also exhibit a hint of the two hotspots, but with much less occurrences than the SE-type drought. Here, we only analyse SE-type super drought for its detection and attribution.

In order to verify the two hotspots identified by the super drought metric, we sought to re-extract them through independent GLDAS soil moisture records. In order to be spatially comparable, the soil moisture data have been standardized to the normal distribution, analogous to SPEI. Accordingly, the severe soil moisture drought is defined as the value less than −1.5. Figure S2 shows the frequency map of severe soil moisture at the layer 10–40 cm, while the patterns for other layers are similar and thus not depicted. It can be found that the results based on soil moisture at 10–40 cm confirm the two super drought hotspots with one located in TCZ and the other in SEA during the recent decades.

Finally, we would like to explain why no significant drought signatures are manifested in the north China, which has been widely recognized as drought prone area (Zhang *et al*., 2017). On the one hand, the subject of this study is super drought regarded as compound water deficits in all parts of usable water resources, rather than the traditional severe drought. When we treat multiscalar drought in isolation, as shown in the complementary Figure S3, the north China has been harassed by severe event with respect to each individual time scale. However, the droughts are not simultaneous and thus the aggregate impact is likely to less severe. On the other hand, either SPEI or soil moisture metric highlights much less drought frequency in north China than in TCZ and SEA (Figures S2 and S3). In summary, the north China is not considered as a drought hotspot.

3.2 | Temporal and seasonal features

Temporal evolutions and seasonal characteristics of the percentage of the land area under super drought over the two hotspots are shown in Figure 2. Over TCZ, from 1960 through the end of 20th century, the areal coverage of super drought is small and rarely exceeded 10%, suggesting almost super drought free status. However, beginning in 2000, roughly 20 to 50% of the TCZ has experienced super drought conditions multiple times. The seasonal dependence of super drought occurrence over TCZ is shown in boxplots (Figure 2b). On the one hand, nearly 67% of the events occurred in summer and autumn, while only 13% occurred in winter. On the other hand, the spatial extent is comparable for spring, summer and autumn, while there has been only a negligible influence during winter. In addition, the "outliers" in the boxplot represent the most expansive events that are all recorded in the recent two decades without exception.

The SEA counterpart is shown in Figure 2c,d. The period around 1990 and the recent decade saw the most widespread and frequent super drought, while other episodes had substantially less area affected. Unlike what happens over the TCZ, the super droughts in SEA are much less active around 2000. In terms of the seasonal behaviours (Figure 2d), it can be seen that the seasonal distribution of the super drought number over SEA bears strong resemblance to that over TCZ, with the largest contribution from summer (34%) followed by autumn (32%) and then spring (17%) and winter (17%). However, spatial coverage for all four seasons becomes more comparable in SEA than in TCZ. In addition, as indicated by the "outliers" of the boxplot, 10 out of 16 super cases over SEA take place in the last two decades.

4 | ATTRIBUTION ANALYSIS OF SUPER DROUGHT

4.1 | Relative role of precipitation and PET

Deficit in precipitation and enhanced evaporation are the two root factors controlling super drought. Thereby, we first aim to separate the role of precipitation and PET in super drought. The contribution of precipitation is calculated by holding PET as its climatological annual cycle, the residue between the raw and precipitation-induced values represents the PET effect. Figure 3 shows the contribution of precipitation and PET to the super drought during the six consecutive decades. As indicated by Figure 3a, in the last 20 years when super drought in TCZ persists, the PET plays a dramatic role, contributing

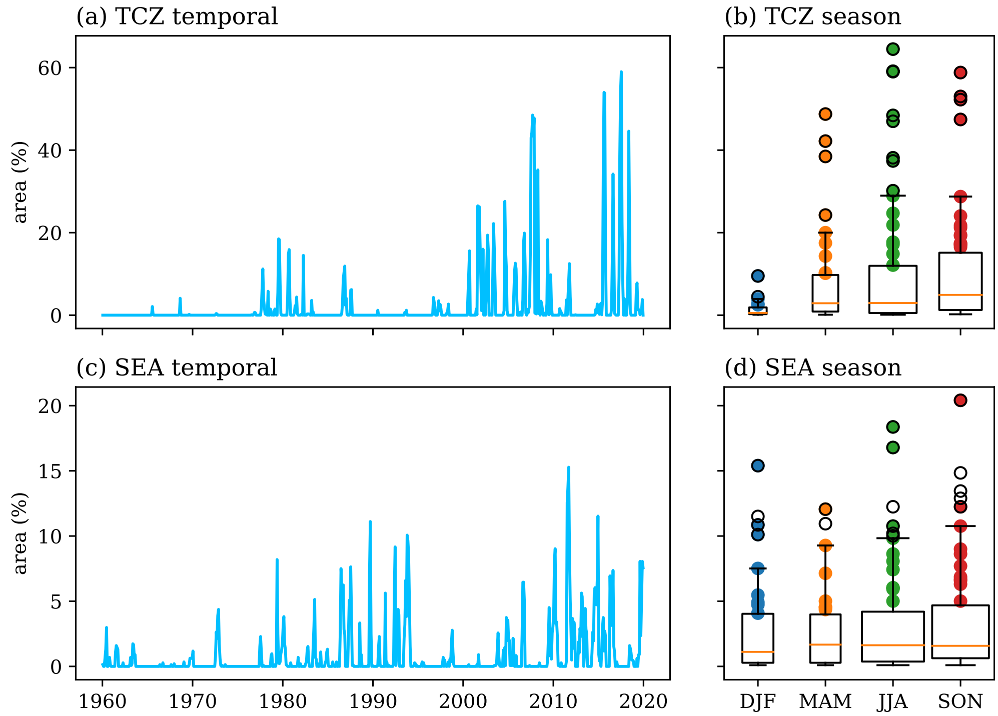

FIGURE 2 (a, c) Temporal evolutions of the percentage of the land area under super drought over TCZ and SEA from 1960 to 2019. (b, d) Boxplots of super-drought affected area percentage for the four seasons (DJF, MAM, JJA and SON). Each boxplot includes median (orange line), the lower and upper quartile (the box), the outer range (1.5 times the interquartile range, shown by the whiskers) and the extremes (black circles). Meanwhile, data points for 2000–2019 greater than upper quartile are overlaid on the boxplot (coloured dots). Note that zero values are not counted to construct boxplot, and the box width is proportional to the sample size [Colour figure can be viewed at wileyonlinelibrary.com]

41% and 80% in the first and second 10 years, respectively. Different from TCZ harbouring a semi-arid climate, the SEA region is situated in monsoon humid zone, where PET makes an overall small contribution of less than 20% (Figure 3b-d). That is, the precipitation rather than PET is the most influential in governing super droughts over SEA. The only exception is noted in SWC for the last decade, with PET making a half contribution.

4.2 | Contribution of decadal variability and trend

As we know, long-term trend in response to global warming and decadal variation cause an overall climate background and have a large influence on extremes. In this part, therefore, the contribution of decadal variability and trend to super drought will be explored for precipitation (section 4.2.1 and Figure 4) and PET (section 4.2.2 and Figure 6), respectively. Behind the precipitation and PET variability, it is well acknowledged that moisture and lift are the two critical ingredients for precipitation, while PET is regulated by temperature, surface net radiation, humidity and wind speed (Allen *et al.*, 1994). In the conclusions and discussions section, we emphasize the need to investigate the physical process acting to regulate precipitation and PET as a future direction of this work.

Note that the attribution analyses for PET are only performed in TCZ and SWC, where PET have significant impacts on super drought in the recent decade. In addition, the trend maps for precipitation and PET for 1960–2019 is shown in Figure S4.

4.2.1 | Precipitation

We apply the EMD to monthly precipitation anomalies after removing the seasonal climatology. While the first five modes represent high frequency oscillations, the sixth and seventh modes represent the decadal and multi-decadal variations, and the final mode denotes the secular trend. The summation of sixth and seventh EMD modes is collectively referred to as decadal variability in this study. The left panel of Figure 4 illustrates the decadal and trend intrinsic modes of precipitation for the TCZ (a) and the three subregions over SEA (b–d). Although

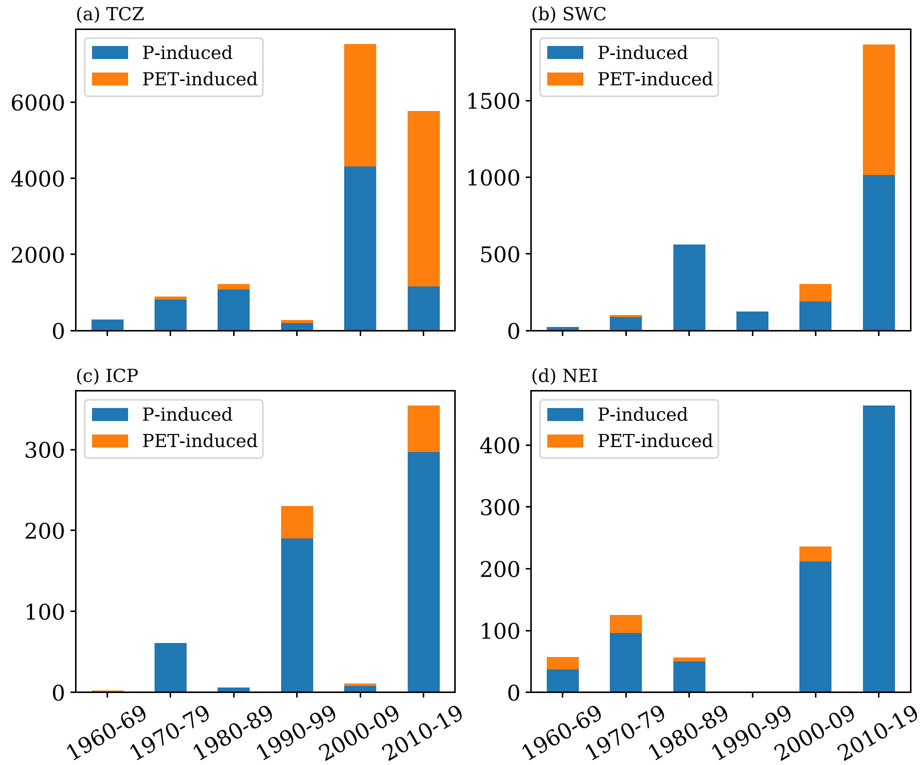

FIGURE 3 Stacked bar charts showing the relative contribution of precipitation (blue) and PET (orange) to super droughts in (a) TCZ, (b) SWC, (c) ICP and (d) NEI. The *x*-axis represents the decades, and *y*-axis total months grids under super drought. Because of the different spatial coverage, the values among the four regions should not be directly compared [Colour figure can be viewed at wileyonlinelibrary.com]

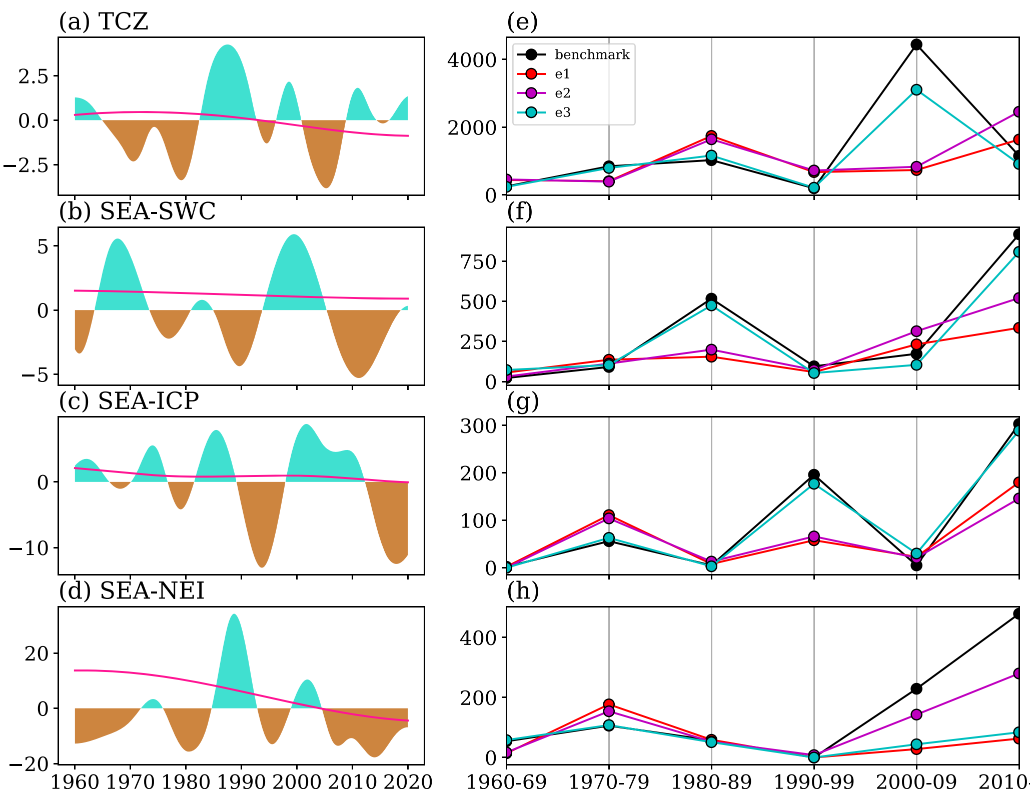

FIGURE 4 (left panel) The decadal (shaded) and trend (lines) EMD modes of precipitation for TCZ and the three subregions over SEA. (right panel) The temporal evolutions of total months grids under super drought calculated with four sets of input data. The four sets of input data include (black) original precipitation, (red) precipitation with both decadal oscillation and trend removed, (purple) precipitation with decadal oscillation removed and (cyan) precipitation with trend removed [Colour figure can be viewed at wileyonlinelibrary.com]

the EMD trend component appears to be in downward direction, only that in NEI has been decreasing in a pronounced manner. As reflected by the spatial pattern of the linear trends for 1960–2019 (Figure S4a), it is confirmed that the linear trends in most parts of East Asia failed statistical test. Contrasting trend component, there is region-wide evidence of strong decadal oscillation, which is more relevant for super drought growth and decay.

As mentioned above, about 57% of prevalent super droughts over TCZ during 2000–2009 is mainly driven by precipitation. This precipitation deficiency is caused by the minimal signal in decadal components, as indicated by Figure 4a. Since 2010, the multidecadal oscillation switched from negative to positive phases, which greatly relieved drought tensions induced by precipitation. However, the enhanced evaporation demand took over as the dominant factor (Figure 3a). Over SEA, it is clear that the recent decade receives the lowest decadal precipitation followed by the period around 1990 (Figure 4b–d), which is responsible for the extensive super droughts shown in Figure 2c.

To obtain a more quantitative evaluation, we keep PET as climatology and remove specific precipitation EMD modes prior to calculating super drought as follows:

(benchmark) original precipitation: pre

(e1) decadal oscillation and trend removed: pre − Imf6 − Imf7 − Imf8
(e2) decadal oscillation removed: pre − Imf6 − Imf7
(e3) trend removed: pre − Imf8

In this way, the difference between benchmark and e2, e3 and e1 shows the contribution from decadal oscillation, trend and their combined effect, respectively. The results are displayed in the right panel of Figure 4.

At TCZ over the entire period except 2000–2009, the results are nearly same regardless whether decadal or trend components are removed or not (Figure 4e). However, the amplitude during 2000–2009 significantly dropped from 4,442 to 833 counts, when ruling out the decadal part. The percentage-based contribution of decadal variation amounts to 85%. In comparative terms, the effect of long-term trend just shifts the magnitude a little.

At SWC and ICP (Figure 4f,g), the trend does not perturb the precipitation-induced super drought occurrence much, but the decadal component exerts large impacts. In the recent decade, about half of the precipitation-induced super drought is attributable to the decadal variability. Such contribution is higher (65–75%) in the period around 1990. Unlike SWC and ICP, decadal variation as well as trend over NEI have contributed equally to the enhanced drying in the recent decade, with the joint contribution as much as 97% (Figure 4h). If the trend and decadal signals both removed, NEI super drought hotspot vanishes. NEI is the only region that presents a non-negligible contribution from trend, in line with significant decreasing tendency at NEI (Figure S4a).

Based on EMD decomposition imposed on observations, we conclude that out of the total variability in precipitation, about half of the super droughts over SEA in the recent decade is caused by decadal variability, while the trend mode has negligible influence. To corroborate above findings, models underpin CMIP6 are used to detect and attribute precipitation changes to anthropogenic and natural causes. Figure 5 shows the temporal changes of ensemble mean in Hist, referred as the forced response, and the range of internal decadal variability depicted as shaded region. As shown in Figure 5a, the internal decadal variability is estimated to be −5.13 to 5.13 mm·month^{-1} and the forced precipitation exceeds the natural variability at around 1977, which is generally consistent with Zhang *et al.* (2021). However, remind that the benchmark used here is the piControl and that it takes about 130 years to exceed the boundary. If we calculate the anomalies relative to the 1960–1999 Hist, as shown in Figure 5b, it can be seen the external forcing induced anomalies in the recent decade is −0.81, which is only 15% of the unforced amplitude. That is to say, in the context of the recent 60 years, the forced signal is appeared to be eclipsed by the decadal variability. Thereby, the model-based result strongly supports the observation-based findings.

Finally, it is necessary to mention that the variance explained by decadal component is typically less than 10%. Therefore, why is the decadal signal substantively important to precipitation-induced super drought changes, as it adds a relatively minor contribution to the total variability? Figure S5 is drawn to address this issue. When comparing the raw series (Figure S5a,c), it is clear that high-frequency mode is one order of magnitude larger that low-frequency mode, with their respective variances being 163 and 10 mm^2. However, remember such result is based on the raw data without regard to cumulative effect. Since drought represents an accumulated precipitation deficit over an extended period of time, especially for long time scale drought, it is indispensable to further examine the cumulative departures and its vibrating amplitude. As indicated by Figure S5b,d, the 24-month aggregation promotes strong signal in decadal mode with variance significantly lifting to 5,894 mm^2. In comparative terms, the 24-month Imf-2 mode has a variance of 1,535 mm^2, falling below the decadal mode (Figure S5e). The reason is straightforward: the longer the aggregation period, the more remarkable the net effect of slow-varying mode. Such result is supported by Wang *et al.* (2019), who had theoretically proved that hydrological drought (long time scale) typically responds to

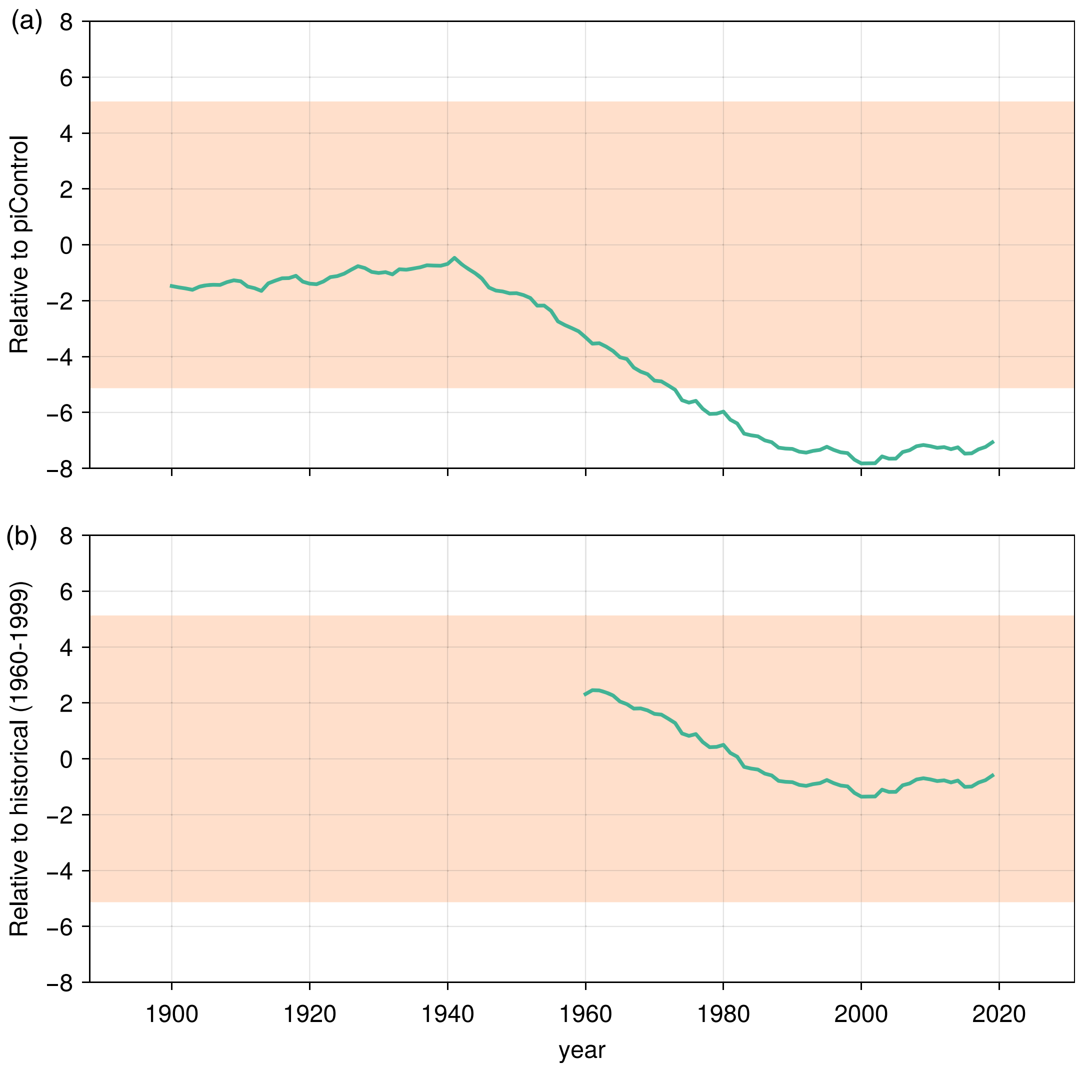

FIGURE 5 The green line shows the changes in anomalous annual precipitation of multimodel ensemble mean in Hist experiment, with the shaded area denoting the internal decadal variability range derived from piControl experiment. The data source for anomalous changes in (a, b) are exactly same, but use different reference periods: (a) piControl and (b) 1960–1999 Hist [Colour figure can be viewed at wileyonlinelibrary.com]

the slowly varying (low frequency) component of precipitation and is insensitive to the components at shorter temporal scales, which have high-frequency oscillations and large variance.

As a concluding remark, the exacerbation of super drought over SEA can be interpreted as decadal precipitation deficit, despite small variance contribution, yielding long-term drought background, which facilitates the overlap with short-term drought and thus super drought.

4.2.2 | Potential evaporation

In the following, the attribution analysis regarding PET-induced super drought is performed over TCZ and SWC regions. Figure 6 shows observed anomalies, EMD trend and decadal components of annual PET. Both TCZ and SWC exhibit an upward PET trend with the linear slope over the entire period of approximately 0.8 mm·decade^{-1}, which exceeds 1% significant level. As shown in Figure S4b, increasing PET are robust over most East Asia, with largest trends occurring in TCZ and SWC. However, these trends are not monotonic, as the PET appears to remain stagnant until 1990, but afterwards it continually increased at the rate of 1.7 mm·decade^{-1}. To what extent is the local PET trend driven by global warming? To address this question, a regression of the local PET trend on the global mean PET trend deduced by EMD as well is performed, and the latter can largely be considered as the forced global warming signal (Stocker, 2014). As indicated by Figure 6, the local PET trend resonates well with variation in the global mean regressed PET. Using the coefficient of determination (R^2)

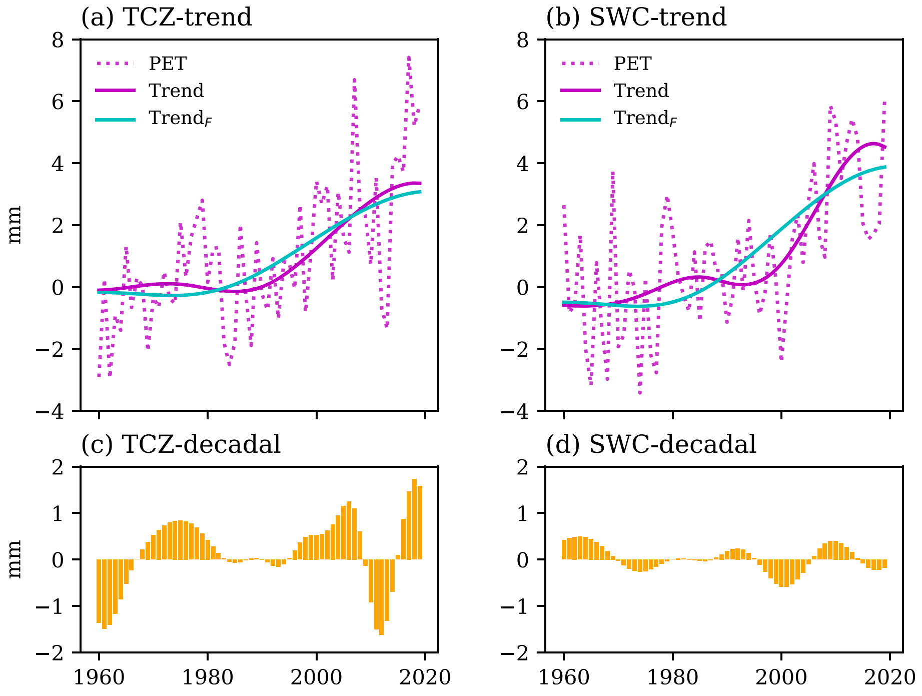

FIGURE 6 (upper panel) The PET anomalies (dotted pink line), the trend component (solid pink line) and the regressed trend component onto the global mean (solid blue line). (bottom panel) The decadal component of the PET. The two columns correspond to TCZ and SWC, respectively [Colour figure can be viewed at wileyonlinelibrary.com]

calculated, the global warming forced signal can explain 92 and 87% of the local trend over TCZ and SEA, respectively. The physical process linking global warming and increased PET is that rising air temperature enhances vapour pressure deficit, which further drives higher evaporative demand.

On decadal variability, the amplitude is rather smaller and it displays mixed weakening and strengthening signals, which tends to negate the net effect. Over TCZ during the 2000–2009, although the decadal component of PET is continuously above the average, the mean magnitude is merely 0.6 mm that is a quarter of the trend amplitude. During the last 10 years, the overall effect of decadal variability is weak over both TCZ and SWC, because of the cancellation signal.

Finally, we integrate model ensembles with observations to re-disentangle the externally and internally forced variability based on Dai *et al.* (2015) method. The method has been documented in section 2.2. The outcome is shown in Figure S6. Overall, the result based on joint model-observation bears a great resemblance to that solely depending on the observation, which provides confidence that the pattern is robust.

5 | CONCLUSIONS AND DISCUSSIONS

In the last decade, a sequence of once-in-50 year or once-in-100 year drought events have hit parts of East Asia, which constitute devastating and far-reaching destructions to agriculture, water availability, ecosystem, economics and society. Motivated by the unprecedented recent super droughts, this study aims to examine the super drought changes over East Asia in the past 60 years, which help put the recent super droughts in the context.

Super droughts in the last 20 years over East Asia have been the most expansive, with two hotspots located in the TCZ and SEA, which together account for 2/3 of the total super droughts. The seasonal distribution characterizes the largest contribution from summer followed by autumn and then spring and winter. Over TCZ in the past 20 years, the significantly rising tendency of PET plays an important role with a contribution of 43 and 80% for the in the first and second 10 years, respectively. Furthermore, the global warming forced signal can explain more than 90% of the local PET trend over TCZ. Over SEA, the recent decade and the period around 1990 saw the most widespread super droughts, and spatial distribution is not uniform but clustered into three subregions. Different from TCZ, the precipitation rather than PET is the most influential in governing super droughts in SEA. Out of the total variability in precipitation, about half of the super droughts in the recent decade is caused by decadal variability, with a percentage contribution of 65–70% in the period around 1990, while the trend mode has negligible influence.

This study elucidates spatiotemporal signatures of super droughts in East Asia and the underlying factors, but much remains to be learned concerning the mechanism. As regards TCZ, the super drought has been most expansive in the recent decade, and we know that the global warming mostly contributes to the PET increase. However, in the 2000–2009, the internally generated decadal precipitation deficit is identified to play the dominant role. Then, what is the physical mechanism responsible? One of the possible reasons is the weakening of East Asian Summer Monsoon (EASM) (Zhou *et al.*, 2009), as a consequence of aerosol forcing that overwhelms the greenhouse gases effects (Song *et al.*, 2014; Li *et al.*, 2015). In addition to examining the EASM itself, the driving forces behind EASM variability, including the thermal forcing of the Tibetan Plateau (Duan *et al.*, 2011; He *et al.*, 2019) and air–sea interaction (Song *et al.*, 2014; He and Zhou, 2020) should also be explored. Another possible reason is the wave-like teleconnection pattern over Eurasia, excited by the SST anomalies over the North Atlantic (Piao *et al.*, 2017). In future work, it is necessary to evaluate the relative role of EASM and mid-latitude circulation in regulating the precipitation in TCZ.

For the unprecedented super drought over SEA in the last decade, we have shown that the decadal shift of precipitation is the most relevant. Our preliminary examination shows that the decadal shift to more super droughts in the recent decade over SEA is probably remotely forced by teleconnection from the Tropical West Indian (TWI) Ocean SST. The key dynamic processes include wedge-shaped Kelvin wave with northeast flank traversing SEA and the vertical circulation cell with ascents over TWI and compensating sinks over SEA. These results will be thoroughly presented in another paper.

ACKNOWLEDGEMENTS

We thank the Editor and the four anonymous reviewers for their time and constructive comments. This work was supported by the National Natural Science Foundation of China (Grants Nos. 41961144016, 41875115, 42175041, 41961144025 and 41831175).

CONFLICT OF INTEREST

The authors declare no potential conflict of interest.

AUTHOR CONTRIBUTIONS

Lin Wang: Conceptualization; formal analysis; investigation; methodology; resources; visualization; writing – original draft. **Wen Chen:** Conceptualization; investigation; resources; validation; writing – review and editing. **Qiang Fu:** Conceptualization; methodology; resources; validation; writing – review and editing. **Gang Huang:** Investigation; methodology; writing – review and editing. **Qiulin Wang:** Software; writing – review and editing. **Chakrit Chotamonsak:** Investigation; writing – review and editing. **Atsamon Limsakul:** Investigation; writing – review and editing.

ORCID

Lin Wang https://orcid.org/0000-0002-3810-4724
Wen Chen https://orcid.org/0000-0001-9327-9079
Gang Huang https://orcid.org/0000-0002-8692-7856
Qiulin Wang https://orcid.org/0000-0001-9113-4546

REFERENCES

Allen, R.G., Smith, M., Pereira, L.S. and Perrier, A. (1994) An update for the calculation of reference evapotranspiration. *ICID Bulletin of the International Commission on Irrigation and Drainage*, 43, 35–92.

Amante, C. and Eakins, B.W. (2009) *ETOPO1 1 arc-minute global relief model: procedures, data sources and analysis*. Boulder, Colorado: National Geophysical Data Center, NOAA. NOAA Technical Memorandum NESDIS NGDC-24.

Barriopedro, D., Gouveia, C.M., Trigo, R.M. and Wang, L. (2012) The 2009/10 drought in China: possible causes and impacts on vegetation. *Journal of Hydrometeorology*, 13(4), 1251–1267.

Beaudoing, H. and Rodell, M. (2019) *GLDAS Noah Land Surface Model L4 monthly 0.25×0.25 degree, Version 2.0*. Greenbelt, Maryland: NASA/GSFC/HSL.

Beaudoing, H. and Rodell, M. (2020) *GLDAS Noah Land Surface Model L4 monthly 0.25×0.25 degree, Version 2.1*. Greenbelt, Maryland: NASA/GSFC/HSL.

Beguería, S., Vicente-Serrano, S.M., Reig, F. and Latorre, B. (2014) Standardized precipitation evapotranspiration index (SPEI) revisited: parameter fitting, evapotranspiration models, tools, datasets and drought monitoring. *International Journal of Climatology*, 34(10), 3001–3023.

Chen, H., He, D. and Zhu, Z. (2019b) The internal multidecadal variability of SST in the Pacific and its impact on air temperature and rainfall over land in the Northern Hemisphere. *Atmosphere*, 10(3), 153.

Chen, H. and Sun, J. (2017) Anthropogenic warming has caused hot droughts more frequently in China. *Journal of Hydrology*, 544, 306–318. https://doi.org/10.1016/j.jhydrol.2016.11.044.

Chen, W., Feng, J. and Wu, R. (2013) Roles of ENSO and PDO in the link of the East Asian winter monsoon to the following summer monsoon. *Journal of Climate*, 26(2), 622–635. https://doi.org/10.1175/JCLI-D-12-00021.1.

Chen, W., Wang, L., Feng, J., Wen, Z., Ma, T., Yang, X. and Wang, C. (2019a) Recent progress in studies of the variabilities and mechanisms of the East Asian monsoon in a changing climate. *Advances in Atmospheric Sciences*, 36(9), 887–901. https://doi.org/10.1007/s00376-019-8230-y.

Dai, A., Fyfe, J. C., Xie, S. P. and Dai, X. (2015) Decadal modulation of global surface temperature by internal climate variability. *Nature Clim Change*, 5, 555–559.

Ding, T. and Gao, H. (2020) The record-breaking extreme drought in Yunnan Province, southwest China during spring-early summer of 2019 and possible causes. *Journal of Meteorological Research*, 34(5), 997–1012. https://doi.org/10.1007/s13351-020-0032-8.

Duan, A., Li, F., Wang, M. and Wu, G. (2011) Persistent weakening trend in the spring sensible heat source over the Tibetan Plateau and its impact on the Asian summer monsoon. *Journal of Climate*, 24, 5671–5682. https://doi.org/10.1175/JCLI-D-11-00052.1.

Feng, S. and Fu, Q. (2013) Expansion of global drylands under a warming climate. *Atmospheric Chemistry and Physics*, 13(19), 10081–10094. https://doi.org/10.5194/acp-13-10081-2013.

Food and Agricultural Organization of the United Nations (FAO). (2017) *Special report: FAO/WFP crop and livestock assessment mission to Mongolia*. Rome, Italy: FAO.

Frankignoul, C., Gastineau, G. and Kwon, Y.-O. (2017) Estimation of the SST response to anthropogenic and external forcing and its impact on the Atlantic Multidecadal Oscillation and the Pacific Decadal Oscillation. *Journal of Climate*, 30(24), 9871–9895.

Fu, Q. and Feng, S. (2014) Responses of terrestrial aridity to global warming. *Journal of Geophysical Research: Atmospheres*, 119(13), 7863–7875. https://doi.org/10.1002/2014JD021608.

Guan, X., Ma, J., Huang, J., Huang, R., Zhang, L. and Ma, Z. (2019) Impact of oceans on climate change in drylands. *Science China Earth Sciences*, 62(6), 891–908. https://doi.org/10.1007/s11430-018-9317-8.

Harris, I., Osborn, T.J., Jones, P. and Lister, D. (2020) Version 4 of the CRU TS monthly high-resolution gridded multivariate climate dataset. *Scientific Data*, 7(1), 109. https://doi.org/10.1038/s41597-020-0453-3.

Hayes, M., Svoboda, M., Wall, N. and Widhalm, M. (2011) The Lincoln declaration on drought indices: universal meteorological drought index recommended. *Bulletin of the American Meteorological Society*, 92(4), 485–488. https://doi.org/10.1175/2010BAMS3103.1.

He, C., Wang, Z., Zhou, T. and Li, T. (2019) Enhanced latent heating over the Tibetan Plateau as a key to the enhanced East Asian summer monsoon circulation under a warming climate. *Journal of Climate*, 32, 3373–3388. https://doi.org/10.1175/JCLI-D-18-0427.1.

He, C. and Zhou, W. (2020) Different enhancement of the East Asian summer monsoon under global warming and interglacial epochs simulated by CMIP6 models: role of the subtropical high. *Journal of Climate*, 33(22), 9721–9733. https://doi.org/10.1175/JCLI-D-20-0304.1.

Huang, J., Yu, H., Guan, X., Wang, G. and Guo, R. (2016) Accelerated dryland expansion under climate change. *Nature Climate Change*, 6(2), 166–171.

Huang, N.E., Shen, Z., Long, S.R., Wu, M.C., Shih, H.H., Zheng, Q., Yen, N.C., Tung, C.C. and Liu, H.H. (1998) The empirical mode decomposition and the Hilbert spectrum for nonlinear and non-stationary time series analysis. *Proceedings of the Royal Society of London. Series A: Mathematical, Physical and Engineering Sciences*, 454, 903–995. https://doi.org/10.1098/rspa.1998.0193.

Li, H., Chen, H., Sun, B., Wang, H. and Sun, J. (2020) A detectable anthropogenic shift toward intensified summer hot drought events over northeastern China. *Earth and Space Science*, 7, e2019EA000836. https://doi.org/10.1029/2019EA000836.

Li, X., Ting, M., Li, C. and Henderson, N. (2015) Mechanisms of Asian summer monsoon changes in response to anthropogenic forcing in CMIP5 models. *Journal of Climate*, 28, 4107–4125. https://doi.org/10.1175/JCLI-D-14-00559.1.

Li, Y., Xu, H. and Liu, D. (2011) Features of the extremely severe drought in the east of southwest China and anomalies of atmospheric circulation in summer 2006. *Acta Meteorologica Sinica*, 25(2), 176–187. https://doi.org/10.1007/s13351-011-0025-8.

Ma, S., Zhou, T., Stone, D.A., Polson, D., Dai, A., Stott, P.A., von Storch, H., Qian, Y., Burke, C., Wu, P., Zou, L. and Ciavarella, A. (2017) Detectable anthropogenic shift toward heavy precipitation over eastern China. *Journal of Climate*, 30, 1381–1396. https://doi.org/10.1175/JCLI-D-16-0311.1.

McKee, T. B., Doesken, N. J. & Kleist, J. (1993). The relationship of drought frequency and duration to timescales. Paper presented at 8th Conference on Applied Climatology, Anaheim, CA, 17–22 January.

Parida, B.R. and Oinam, B. (2015) Unprecedented drought in north-east India compared to western India. *Current Science*, 109, 2121–2126.

Piao, J., Chen, W., Wei, K., Liu, Y., Graf, H.-F., Ahn, J.-B. and Pogoreltsev, A. (2017) An abrupt rainfall decrease over the Asian inland plateau region around 1999 and the possible underlying mechanism. *Advances in Atmospheric Sciences*, 34(4), 456–468. https://doi.org/10.1007/s00376-016-6136-5.

Rodell, M., Houser, P. R., Jambor, U., Gottschalck, J., Mitchell, K., Meng, C. J., Arsenault, K., Cosgrove, B., Radakovich, J., Bosilovich, M., Entin, J. K., Walker, J. P., Lohmann, D. and Toll, D. (2004) The Global Land Data Assimilation System. *Bulletin of the American Meteorological Society*, 85, 381–394. https://doi.org/10.1175/BAMS-85-3-381

Sherwood, S. and Fu, Q. (2014) Climate change. A drier future? *Science*, 343(6172), 737–739. https://doi.org/10.1126/science.1247620.

Song, F., Zhou, T. and Qian, Y. (2014) Responses of East Asian summer monsoon to natural and anthropogenic forcings in the 17 latest CMIP5 models. *Geophysical Research Letters*, 41, 596–603. https://doi.org/10.1002/2013GL058705.

Spinoni, J., Barbosa, P., Bucchignani, E., Cassano, J., Cavazos, T., Christensen, J.H., Christensen, O.B., Coppola, E., Evans, J., Geyer, B., Giorgi, F., Hadjinicolaou, P., Jacob, D., Katzfey, J., Koenigk, T., Laprise, R., Lennard, C.J., Kurnaz, M.L., Li, D., Llopart, M., McCormick, N., Naumann, G., Nikulin, G., Ozturk, T., Panitz, H.J., Porfirio da Rocha, R., Rockel, B., Solman, S.A., Syktus, J., Tangang, F., Teichmann, C., Vautard, R., Vogt, J.V., Winger, K., Zittis, G. and Dosio, A. (2020) Future global meteorological drought hot spots: a study based on CORDEX data. *Journal of Climate*, 33(9), 3635–3661.

Stocker, T. (2014) *Climate Change 2013: The Physical Science Basis: Working Group I Contribution to the Fifth Assessment Report of the Intergovernmental Panel on Climate Change*. New York, NY: Cambridge University Press.

Sun, S., Li, Q., Li, J., Wang, G., Zhou, S., Chai, R., Hua, W., Deng, P., Wang, J. and Lou, W. (2019) Revisiting the evolution of the 2009–2011 meteorological drought over southwest China. *Journal of Hydrology*, 568, 385–402. https://doi.org/10.1016/j.jhydrol.2018.10.071.

Torres, M.E., Colominas, M.A., Schlotthauer, G. and Flandrin, P. (Eds.). (2011) *A Complete Ensemble Empirical Mode Decomposition with Adaptive Noise*. Prague, Czech Republic: IEEE.

UN Office for Disaster Risk Reduction. (2020) *The human cost of disasters—an overview of the last 20 years 2000–2019*. Geneva, Switzerland: UN Office for Disaster Risk Reduction.

United Nations ESCAP. (2019) *Ready for the dry years building resilience to drought in Southeast Asia*. Bangkok, Thailand: United Nations ESCAP.

Vicente-Serrano, S.M., Beguería, S. and López-Moreno, J.I. (2010) A multiscalar drought index sensitive to global warming: the standardized precipitation evapotranspiration index. *Journal of Climate*, 23(7), 1696–1718. https://doi.org/10.1175/2009JCLI2909.1.

Vicente-Serrano, S.M., van der Schrier, G., Beguería, S., Azorin-Molina, C. and Lopez-Moreno, J.-I. (2015) Contribution of precipitation and reference evapotranspiration to drought indices under different climates. *Journal of Hydrology*, 526, 42–54.

Wang, L. and Chen, W. (2014) A CMIP5 multimodel projection of future temperature, precipitation, and climatological drought in China. *International Journal of Climatology*, 34(6), 2059–2078. https://doi.org/10.1002/joc.3822.

Wang, L., Chen, W., Huang, G. and Zeng, G. (2017) Changes of the transitional climate zone in East Asia: past and future. *Climate Dynamics*, 49(4), 1463–1477. https://doi.org/10.1007/s00382-016-3400-4.

Wang, L., Chen, W. and Zhou, W. (2014) Assessment of future drought in southwest China based on CMIP5 multimodel projections. *Advances in Atmospheric Sciences*, 31, 1035–1050. https://doi.org/10.1007/s00376-014-3223-3.

Wang, L., Chen, W., Zhou, W. and Huang, G. (2015) Drought in southwest China: a review. *Atmospheric and Oceanic Science Letters*, 8(6), 339–344.

Wang, L., Chen, W., Zhou, W. and Huang, G. (2016) Understanding and detecting super-extreme droughts in southwest China through an integrated approach and index. *Quarterly Journal of the Royal Meteorological Society*, 142(694), 529–535. https://doi.org/10.1002/qj.2593.

Wang, L., Huang, G. and Chen, W. (2019) Towards a theoretical understanding of multiscalar drought indices based on the relationship between precipitation and standardized precipitation index. *Theoretical and Applied Climatology*, 136, 1465–1473. https://doi.org/10.1007/s00704-018-2578-2.

Wang, Q., Wang, L., Huang, G., Piao, J. and Chotamonsak, C. (2020) Temporal and spatial variation of the transitional climate zone in summer during 1961–2018. *International Journal of Climatology*, 41(3), 1633–1648.

Wang, S., Huang, J. and Yuan, X. (2021) Attribution of 2019 extreme spring–early summer hot drought over Yunnan in southwestern China. *Bulletin of the American Meteorological Society*, 102(1), S91–S96. https://doi.org/10.1175/BAMS-D-20-0121.1.

Wang, W., Zhou, W., Wang, X., Fong, S.K. and Leong, K.C. (2013) Summer high temperature extremes in southeast China associated with the East Asian jet stream and circumglobal teleconnection. *Journal of Geophysical Research: Atmospheres*, 118(15), 8306–8319. https://doi.org/10.1002/jgrd.50633.

World Meteorological Organization. (2006) *Drought Monitoring and Early Warning: Concepts, Progress, and Future Challenges*, Vol. 1006. Geneva: World Meteorological Organization.

Wu, Z. and Huang, N.E. (2009) Ensemble empirical mode decomposition: a noise-assisted data analysis method. *Advances in Adaptive Data Analysis*, 1(1), 1–41. https://doi.org/10.1142/S1793536909000047.

Zhang, L., Chen, Z. and Zhou, T. (2021) Human influence on the increasing drought risk over Southeast Asian monsoon region. *Geophysical Research Letters*, 48, e2021GL09377.

Zhang, L., Wu, P. and Zhou, T. (2017) Aerosol forcing of extreme summer drought over north China. *Environmental Research Letters*, 12, 34020. https://doi.org/10.1088/1748-9326/aa5fb3.

Zhang, L. and Zhou, T. (2015) Drought over East Asia: a review. *Journal of Climate*, 28(8), 3375–3399. https://doi.org/10.1175/JCLI-D-14-00259.1.

Zhang, L., Zhou, T., Chen, X., Wu, P., Christidis, N. and Lott, F.C. (2020) The late spring drought of 2018 in south China. *Bulletin of the American Meteorological Society*, 101, S59–S64. https://doi.org/10.1175/BAMS-D-19-0202.1.

Zhao, T. and Dai, A. (2017) Uncertainties in historical changes and future projections of drought. Part II: model-simulated historical and future drought changes. *Climatic Change*, 144(3), 535–548. https://doi.org/10.1007/s10584-016-1742-x.

Zhou, T., Gong, D., Li, J. and Li, B. (2009) Detecting and understanding the multi-decadal variability of the East Asian summer monsoon recent progress and state of affairs. *Meteorologische Zeitschrift*, 18, 455–467. https://doi.org/10.1127/0941-2948/2009/0396.

SUPPORTING INFORMATION

Additional supporting information may be found in the online version of the article at the publisher's website.

How to cite this article: Wang, L., Chen, W., Fu, Q., Huang, G., Wang, Q., Chotamonsak, C., & Limsakul, A. (2022). Super droughts over East Asia since 1960 under the impacts of global warming and decadal variability. *International Journal of Climatology*, *42*(9), 4508–4521. https://doi.org/10.1002/joc.7483